Effect of Coaxial Electrode Geometry on the Electric Field Enhancement Factor for a High Voltage Vacuum Gap

S. W. Cordaro, S. C. Bott-Suzuki, *Senior Member, IEEE*, J. Banasek, and Tobias Oliver

***Abstract*— We present an experimental analysis of the change in the electric field enhancement factor with varying gap size and penetration depth (P.D) of cathode into anode for a coaxial vacuum gap, diagnosed using Fowler–Nordheim analysis and optical imaging via scanning electron microscope (SEM) and time integrated Digital single lens reflex camera (DSLR). Data were collected on the Coaxial Gap Breakdown Machine (240 A, 25 kV, 150 ns, ∼0.1 Hz). Experiments using five different gap sizes at nine different P.Ds are compared over runs comprising 50 shots for each case. The results show a strong link between enhancement factor and gap size, with P.D and surface topology. For large gap sizes, 150, 330, and 700 μm, the average enhancement factor value increases with increasing P.D. For smaller gap sizes, 50 and 100 μm, the average enhancement factor decreases with P.D. SEM imaging before and after plasma formation for each gap size allows for quantifying surface finish, microprotrusion growth, average blast diameter, and an estimation of the surface area breakdowns occupy. Time integrated DSLR imaging analysis of the gap at each shot allows for a determination of the distribution of breakdowns about the circumference of the gap for each case tested. The Fowler–Nordheim analysis allows for a quantitative analysis of the surface roughness of all gap sizes tested. Results show that for large gap sizes, the gap geometry and increasing area of breakdown is the main cause for increasing average enhancement factor. For small gap sizes, the dominant driving factor for small average enhancement factors—that subsequently decrease with P.D—is significant changes in surface topology due to an increased number of breakdowns.**

***Index Terms*— Electron emission, plasma devices, vacuum arcs, vacuum breakdown.**

I. Introduction

VACUUM gap breakdown at high voltages, typically in the range of tens of kilovolts to megavolts, occurs in many systems, particularly where high current conduction is required. Several standard geometries, such as sphere-sphere, plane-plane, and point-plane, have been extensively investigated under both pulsed and dc conditions and, in general, are well understood and documented [1]–[4]. To date, little detailed analysis of explosive emission in coaxial geometry has been performed, although this geometry is a common feature of high energy devices, including vacuum transmission lines and switch systems. The present work is motivated by the need to better understand the mechanisms by which breakdown initiation occurs in a coaxial gap over a few nanoseconds to a few microseconds at tens of kilovolt at gap sizes of up to 1 mm. Of specific interest is how changes in gap size and penetration depth (P.D) of cathode into anode effect the initiation of breakdowns about the azimuth as represented by the enhancement factor (β). Here, P.D is the distance over which the solid cylindrical cathode is inserted into the hollow cylindrical anode (Fig. 1). Our previous work [5] has shown a link between increasing enhancement factor and current density distribution about the azimuth, as well as showing that asymmetry in breakdown initiation about the azimuth leads to persistent asymmetry in current density distribution. The cause of this increased enhancement factor, and thus redistribution has yet to be studied. This is particularly interesting when considering one mounting system for Sandia's MagLIF [6] (∼20–26 MA) design maintains a coaxial vacuum gap (∼25 μm) in the power feed as the machine voltage is applied. Here, we will use the electric field enhancement factor obtained from the Fowler–Nordheim [7] I–V curve and optical imaging data to determine the behavior of breakdowns in a coaxial gap.

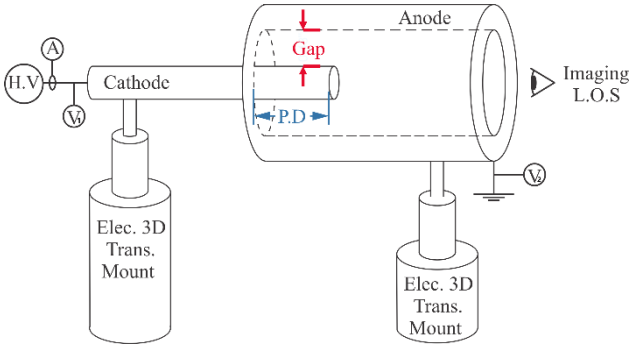

Fig. 1. Diagram of electrode geometry of the CGB machine. Electrodes are 46 mm in length and vary in radius to form the gap as labeled in red. Blue is the P.D which varies from 1.5 to 8.5 mm. The electrodes are monitored by current (A) and voltage (V_1 and V_2) probes and mounted on electrical 3-D translational mounts. Time gated optical imaging is along the imaging line of sight as denoted by the eye.

Manuscript received 16 August 2021; revised 3 January 2022, 22 February 2022, and 13 April 2022; accepted 11 May 2022. Date of publication 27 May 2022; date of current version 13 July 2022. This work was supported in part by the National Nuclear Security Administration (NNSA) Stockpile Stewardship Academic Alliance (SSAA) Program through the Department of Energy (DOE) Cooperative Agreement under Grant DEFC03-02NA00057 and in part by the Sandia National Laboratories under Contract 2004104. The review of this article was arranged by Senior Editor S. J. Gitomer. *(Corresponding author: S. W. Cordaro.)*

The authors are with the Center for Energy Research, University of California San Diego, La Jolla, CA 92093 USA (e-mail: scordaro@ucsd.edu).

Color versions of one or more figures in this article are available at https://doi.org/10.1109/TPS.2022.3176008.

Digital Object Identifier 10.1109/TPS.2022.3176008

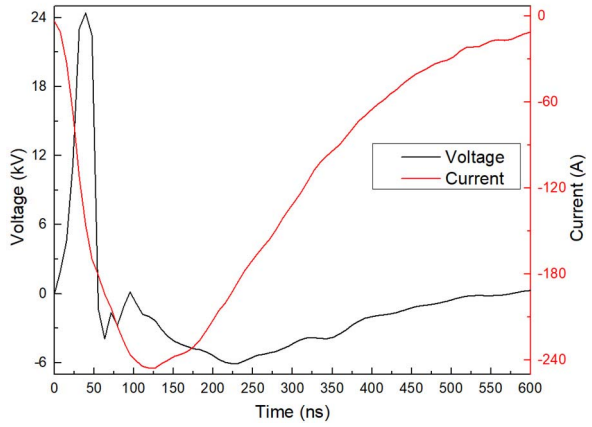

Fig. 2. Typical current (red) and voltage (black) profiles of the CGB machine.

II. Experimental Design and Analysis Methods

An experimental system was previously developed to study breakdown mechanisms and influences of coaxial geometry vacuum gaps [5]. This tabletop experiment, the coaxial gap breakdown (CGB) machine, consists of two aluminum alloy (5056) electrodes; a hollow cylinder of fixed inner diameter (∼18.5 mm) with an inserted solid cylinder. Both are attached to electrical 3-D translational mounts to ensure the electrodes are parallel to one another, and to control their relative positions (Fig. 1). This coupled with electrical continuity testing after alignment and breakdown position distribution calculations ensures that electrodes are centered with a defined gap. Electrodes can be readily machined to create any azimuthal gap required in the coaxial geometry, 25 μm to several millimeters. In this study of over 2000 shots, we examine five azimuthal gap sizes (50, 100, 150, 300, and 700 μm) and P.Ds of the central conductor into the hollow (outer) electrode from 1.5 to 8.5 mm. Prior to changing P.D, the cathode is changed, and the anode is cleaned. It is important to note that while the electrodes used for this work are cleaned with alcohol following machining, they are not polished or treated further. The typical surface roughness of the anode and cathodes [Fig. 8(a)] is 5–10 μm as determined by scanning electron microscope (SEM) imaging.

Experiments were performed under vacuum ($<10^{-5}$ torr) and at room temperature. A high-voltage pulse (25 kV) is delivered *via* a charge circuit to the coaxial gap driving 240 A (125 ns to peak) through the gap, a typical current and voltage trace can be seen in Fig. 2. The device is repetition rated at 0.1 Hz, which allows for statistical analysis to be performed, with the examination of each gap size of P.D comprising 50 shots. The time between shots ensures that the electrodes are considered to be cold before the next shot. The vacuum gap was monitored electrically by Pearson coil (model 6585, 1.5-ns rise time), and by a pair of high-voltage probes (Pintek-HVP-39 pro, 1.6-ns rise time, V_1 and V_2) located at the high voltage and ground sides of the electrodes (Fig. 1). Optically, the gap is monitored *via* time integrated digital single lens reflex camera (DSLR) that takes an image of the coaxial gap (20-μm spatial resolution) along the imaging line of sight for each shot.

The recovered electrical data on every shot allows for the characterization of the breakdown process through the use of the Fowler–Nordheim equation [7] [see (1)]

$$J = \frac{e^3 E^2}{8\pi h \phi t^2(y)} \exp\left[\frac{-4(2m)^{\frac{1}{2}}\phi^{\frac{3}{2}} f(y)}{3\hbar e E}\right]. \tag{1}$$

J is the emission current density, E is the applied electric field, and ϕ is the emitter work function. The functions $t^2(y)$ and $f(y)$ are as follows:

$$y = 3.79x10^{-4}\frac{E^{\frac{1}{2}}}{\phi}$$
$$f(y) = 0.95 - y^2$$
$$t^2(y) \approx 1.1.$$

Equation (1) can be transformed [8], [9] in order to be used experimentally *via* a simple substitution of

$$J = I/A \tag{2}$$
$$E = \beta V/d \tag{3}$$

where A is an area factor, d is the size of the vacuum gap, and β is the electric field enhancement factor, which is the increase of an electric field on the surface of a conductor due to the geometry of the emitters on the surface [10]. These parameters can be evaluated directly by plotting $\ln(I/V^2)$versus$1/V$, where V and I are the experimentally measured voltage and current, respectively. The resulting graph yields a straight line, with a slope (S) [8], [9] of

$$I - -V\text{slope} \equiv S = -2.83x10^7\phi^{\frac{3}{2}}\frac{d}{\beta} \tag{4}$$

that varies for each respective shot, geometry, and material.

If we then say the work function (ϕ) is constant for our electrode material, we can solve for the enhancement factor with respect to slope

$$\beta = -2.83x10^7\phi^{\frac{3}{2}}\frac{d}{S}. \tag{5}$$

We can then directly examine how the enhancement factor (β) changes on average with increasing P.D (Figs. 5 and 6) and gap size (d). The evaluation of the enhancement factor [see (5)] will allow us to better understand how the characteristics of the surface roughness of the electrode effect the breakdowns about the azimuth change from shot to shot.

With the recovered time integrated optical imaging, we can determine the location of breakdowns that occur in each shot and at each P.D. We do this by converting the image of the coaxial gap [Fig. 3(a)] to gray scale and performing a circular lineout [Fig. 3(b)]. The high intensity peaks of the line out correspond to a breakdown and its location about the azimuth [Fig. 3(c)].

Overlapping this information for 50 shots at a given P.D shows the azimuthal distribution of breakdown over the circumference of the gap. A spread in azimuthal distribution correlates to electrodes that are centered, and a gap that is defined. Alternatively, if the distribution is clustered in a single spot or quadrant in the degree range, the electrodes are not centered, and the gap is not well defined. This is of particular

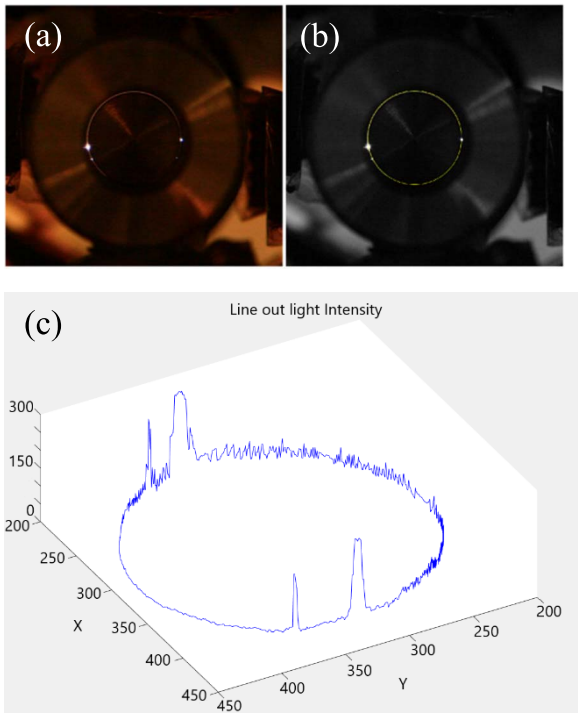

Fig. 3. 150-μm gap, P.D-8.5 mm. (a) Unaltered coaxial time integrated image of a single shot. (b) Gray-scaled version of (a) with a yellow circular lineout across the gap. (c) Intensity peaks and location of the breakdowns about the azimuth.

interest for the smaller gap sizes where ensuring a centered, defined gap can be difficult.

Fig. 4(a) and (b) shows the azimuthal distribution for 50 shots at 100 μm at a P.D of 8.5 mm, and 50 μm at a P.D of 3.34 mm. The data are spread across all quadrants of the gap with small regions having no breakdowns, indicating that the electrodes here are centered and well defined. Fig. 4(c) shows an azimuthal distribution for a 150-μm gap at a P.D of 8.5 mm (50 shots). The data are centered between 195° and 204° with no spread into the other quadrants of the gap, indicating that the cathode is offset in the anode. This qualitative method is used every shot series to ensure the data collected is from electrodes that are centered with a defined gap.

Through the use of an SEM, we are able to image the cathode on the micrometer scale. This imaging allows for a characterization of the surface pre-/post-breakdown initiation and facilitates a discussion of the likely mechanisms responsible for the observed behavior.

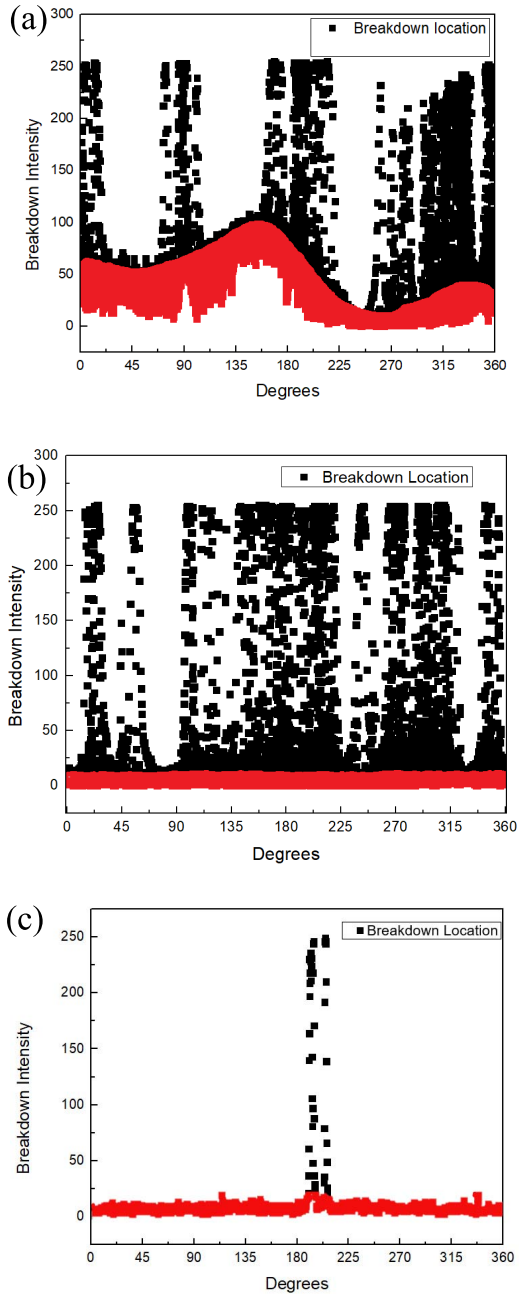

Fig. 4. Breakdown intensity peak locations in degrees for (a) 100-μm gap, P.D-8.5 mm, 50 shots, (b) 50-μm gap, P.D-3.34 mm, 50 shots, and (c) 150-μm gap, P.D-8.5 mm (electrode offset from centered position by 70 μm $\sim$ 180° position). Red highlighted data are background light and are present in every shot. Black data are peak intensity values that each represents an individual breakdown location about the azimuth.

III. Results and Discussion

The Fowler–Nordheim analysis is applied to 2000 shots over five geometries at nine P.Ds. A single shot series for a given geometry and P.D consists of 50 shots whose enhancement factor [see (5)] is then averaged and plotted against P.D.

Fig. 5 shows the enhancement factor for 150-, 300-, and 700-μm gap sizes plotted over increasing P.Ds. At P.D 1.5 mm, we see an enhancement value for 150 μm is 20 and decreases to a value of 10 at a P.D of 2.53 mm. After this point, the enhancement factor increases with increasing P.D and area to a maximum value of 45 at 8.5 mm P.D. The initial decrease and subsequent increase seen here at small P.Ds is believed to be due to the dominance of cathode edge in the gap, where at depths beyond 2.5 mm, the geometry and area of the inserted cathode likely play the dominant role. Similar behavior is seen in the 330 and 700-μm gap size electrodes.

Fig. 6 shows the average enhancement factor versus the P.D for the smallest gap sizes tested, 50 and 100 μm. When looking at the 100 μm gap, at 1.5 mm P.D we see an enhancement factor of 56. This decreases when increasing the P.D to 2.0 mm to a value of 54. When increasing the penetration further than

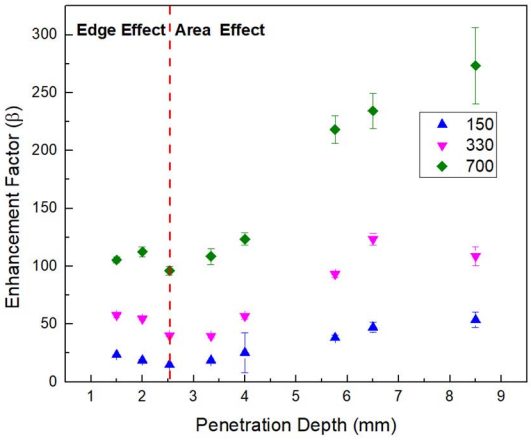

Fig. 5. Average enhancement factor versus P.D for 150-, 300-, and 700-μm gaps. Increasing value with P.D.

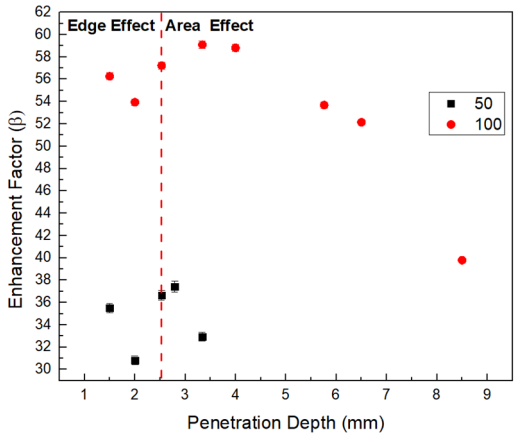

Fig. 6. Average enhancement factor versus P.D for 50- and 100-μm gaps. Decreasing value with P.D.

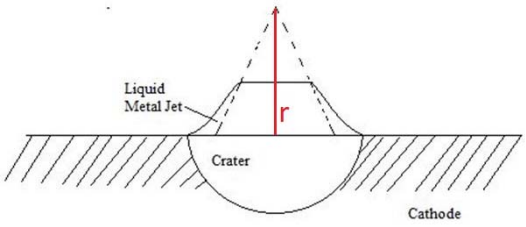

Fig. 7. Microprotrusion transition to liquid jet and crater diagram.

2.5 mm, we see a slight increase in enhancement factor to 60 at 3.34 mm before decreasing to a value of 40 at 8.5 mm. This appears to be a similar to the initial trend seen in the 150, 330, and 700 μm gaps, and is again likely due to the edge effect of the cathode at such a small P.D. However, this decreasing trend continues for all remaining P.Ds past 3.34 mm in the 100 μm gap, and after a P.D of 2.79 mm in the 50-μm gap. The limited number of data points for the 50-μm gap is due to difficulty in ensuring a centered gap at large P.Ds. Future work will quantify the repeatability of the observed behavior for similar gap spacing and P.Ds.

To attempt to understand the behavior demonstrated above, we can consider the electrode surfaces before and after breakdown events. Mesyats [11] describes a process by which

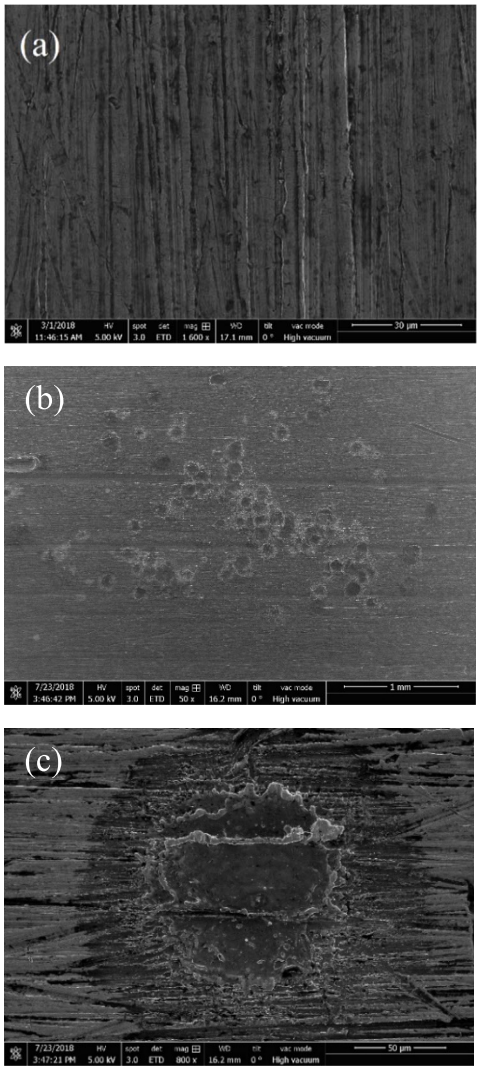

Fig. 8. 700-μm gap (a) before plasma formation (30-μm scale—vertical machining lines) and (b) after plasma formation (1 mm scale—horizontal machining lines) as a result of 50 shots at a P.D-8.5 mm. (c) is a magnification of (b) to 50-μm scale (horizontal machining lines).

breakdowns are enhanced in a vacuum gap by the presence of microprotrusions (emitters). Fig. 7 shows a simple diagram of a microprotrusion, with the dotted line representing the protrusion height (r) before current is passed through the cathode and the solid line afterward. Once current is passed into the cathode, current density increases the temperature of the microprotrusion, such that it eventually melts and ionizes. A portion of the microprotrusion remaining in the melt stage [12], [13] is then explosively propelled into the gap and across the cathode surface, creating additional microprotrusions and leaving behind a crater in the cathode surface. A crater may have a height which varies either above or below the original cathode surface level [14], effectively becoming another microprotrusion. The process occurs at all breakdown positions on the cathode, evidence of which can be imaged *via* SEM [15].

Fig. 8 shows surface imaging for a 700-μm gap cathode. Fig. 8(a) shows an "off the lathe" cathode at a 30-μm scale, with surface imperfections of order 5–10 μm. Fig. 8(b) shows

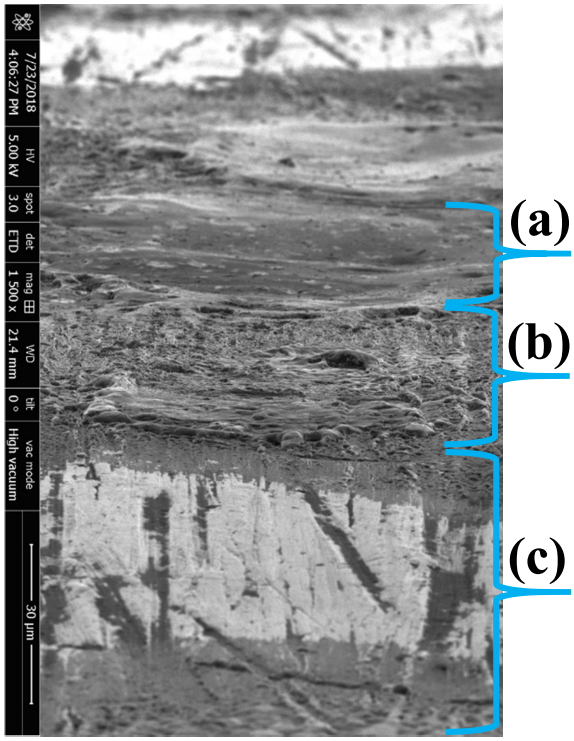

Fig. 9. 700-μm gap side on and rotated $\times$1500 magnification of a breakdown, with (a) smoothed crater zone, (b) molten splash created microprotrusions, and (c) undisturbed electrode surface.

TABLE I

GAP SIZE COMPARED WITH PERCENTAGE OF THE GAP THAT MICROPROTRUSIONS ON THE CATHODE AND ANODE OCCUPY. WITH A MINIMUM PROTRUSION SIZE OF 20 μm (10 μm ON EITHER SIDE) AND 40 μm (20 μm ON EITHER SIDE)

20 (μm) Microprotrusion (cathode + anode)					
Gap size	50 μm	100 μm	150 μm	330 μm	700 μm
Percentage of gap protrusions occupies	40%	20%	13%	6%	3%
40 (μm) Microprotrusion (cathode + anode)					
Gap size	50 μm	100 μm	150 μm	330 μm	700 μm
Percentage of gap protrusions occupies	80%	40%	27%	12%	6%

a postplasma formation at the 1-mm scale. Large craters and clusters of craters resulting from plasma formation can be seen against a background of the original electrode finish. Fig. 8(c) shows a 50-μm scale image of an individual breakdown crater on the surface of the cathode. A blast crater is seen in the image, with nanometer roughness molten material in the center of the crater surrounded by molten build up that forms microprotrusions [11] on the order of 10–20 μm. Fig. 9 shows a side-on SEM image of a breakdown crater for a 700-μm gap cathode. Shown is a [Fig. 9(a)] smooth molten crater that dips below the [Fig. 9(b)] blast created microprotrusions and the [Fig. 9(c)] undisturbed surface. From this image, it

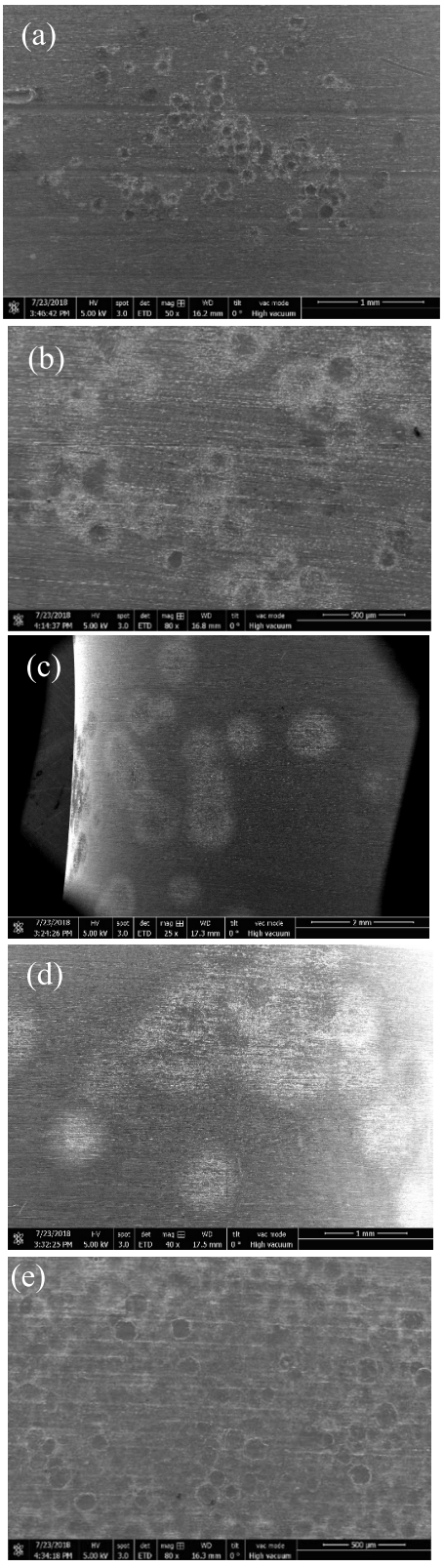

Fig. 10. SEM imaging centered on blast regions for (a) 700 μm, (b) 330 μm, (c) 150 μm, (d) 100 μm, and (e) 50-μm gaps. These are the results of 50 shots for each gap at (a)–(d) P.D-8.5 mm and (e) 3.34 mm.

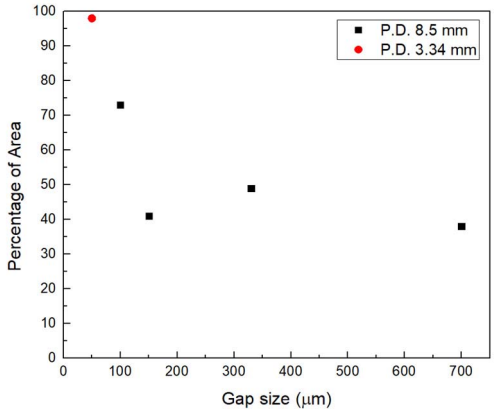

Fig. 11. Average percent area occupied by breakdowns for all gap sizes tested. With black squares showing data collected at P.D-8.5 mm and the red square showing data collected at P.D-3.34 mm.

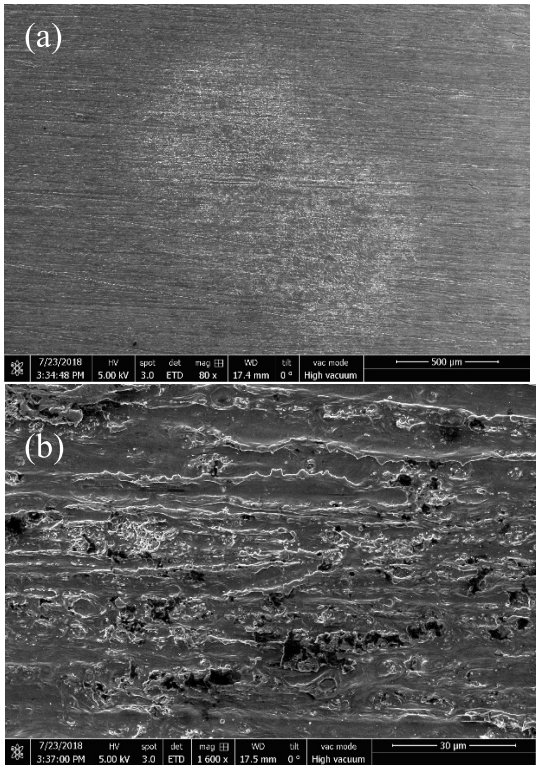

Fig. 12. 100-μm gap centered on a large breakdown at scales of (a) 500 μm and (b) 30 μm.

is clear that new microprotrusions can be formed by blast craters and molten blast buildup caused by plasma breakdown. It is important to note that the craters shown in the SEM images may be the result of a single or large cluster [9] of microprotrusions exploding.

Using SEM imaging and the Mesyats breakdown description, we can investigate potshots information of the surface of our tested electrodes to see how surface features change with changes in gap size. From Fig. 9, we have measured that the microprotrusions are of order 10–20 μm on both anode and cathode, in height only. From this, we can estimate the percentage of the gap that is occupied by individual microprotrusions of this size, while not accounting for anything thing

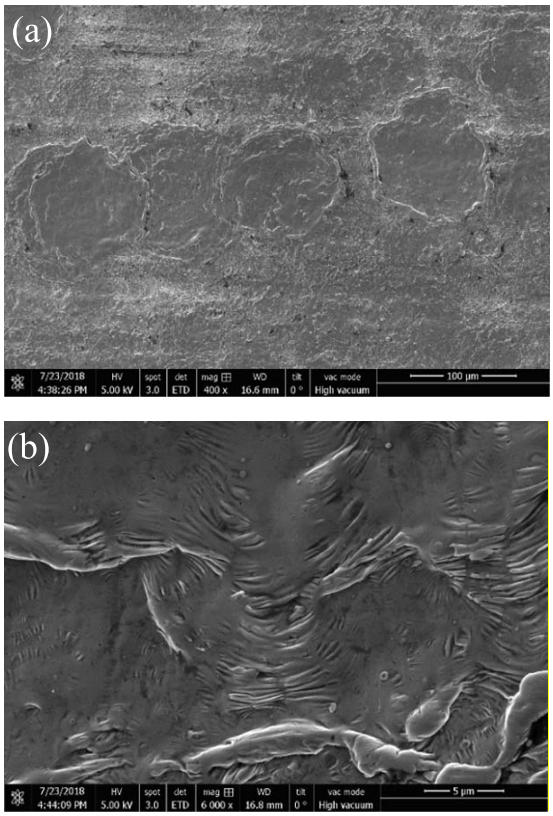

Fig. 13. 50-μm gap centered on large cluster of breakdowns at scales of (a) 100 μm and (b) 5 μm.

else about the microprotrusion geometry. Table I shows that for larger gap sizes, the microprotrusion is a small percentage of the gap. At smaller gap sizes, the percentage of the gap that is filled by the microprotrusions is significantly larger.

SEM surface imaging in Fig. 10 shows a small area of the electrode surface with breakdowns throughout for all gap size cathodes tested. From this, we can measure the average diameter, and thus area of each breakdown deformation, as well as optically count the number of breakdowns visible within the image area. Coupling this information, we can estimate on average what percentage of the total penetrated surface area the breakdown deformations cover (Fig. 11).

Fig. 11 shows the average percent area occupied by breakdowns for all gap sizes tested. It is important to note here that for simplicity, we are assuming that we have no overlap in our breakdown craters so the values presented are higher than would be the case for overlapping craters. The percent of area occupied by the breakdowns for the large gap sizes (700, 330, 150 μm) is between 40% and 50%. The percentage of the area occupied by the breakdowns generally decreases with decreasing blast diameter and increasing gap size [Fig. 10(a)–(c)]. The microprotrusions that do form take up a 3%–27% of the gap (Table I), with the remaining 60%–50% of the surface area being "off the lathe" protrusions of 5–10 μm. For the small gap sizes tested (100, 50 μm), the percentage of the area that breakdowns occupy increases significantly to 70% and 97%, respectively. This large increase is due to the increased number of breakdowns observed in SEM images [Fig. 10(d) and (e)]. The microprotrusions that form occupy

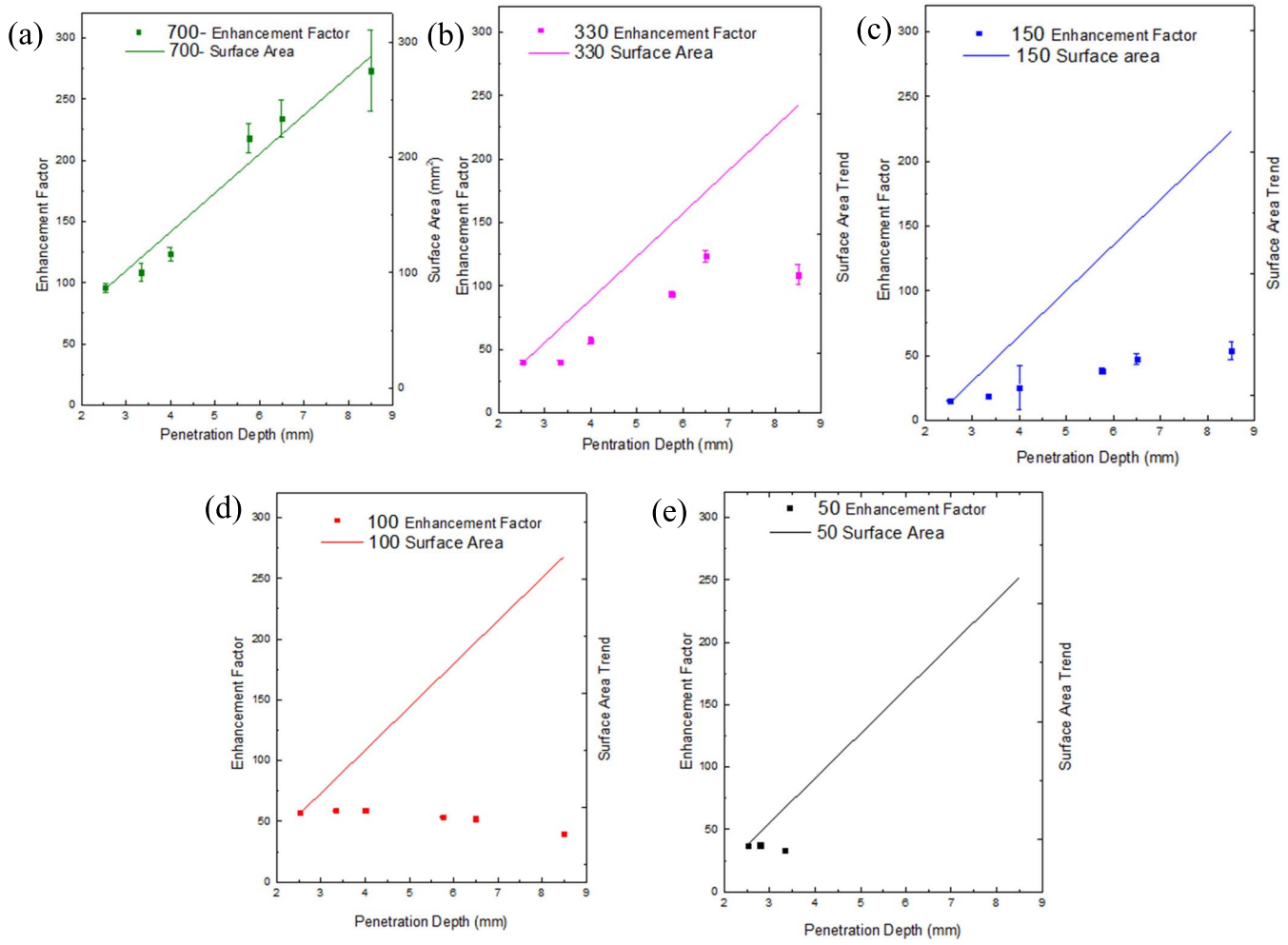

Fig. 14. Electrode surface area and enhancement factor for (a) 700 μm, (b) 330 μm, (c) 150 μm, (d) 100 μm, and (e) 50-μm gaps versus P.D. With the solid lines representing the surface area of the penetrated electrode, and the solid square being the enhancement factor value.

20%–80% of the gap (Table I), with the remaining surface 3%–30% of the surface being "off the lathe" protrusions of 5–10 μm. Furthermore, the surface topology of the breakdowns on the 100- (Fig. 12) and 50-μm (Fig. 13) cathodes is characterized by large overlapping smooth breakdown areas.

Comparing the observed behavior at the surface, *via* SEM imaging, for the gap sizes tested, we can infer which factors are dominant in changing the enhancement factor and driving breakdown. For large gap sizes, we see from surface imaging that the cathode surface is not dominated by the creation or destruction of microprotrusions, and the protrusions that do form from breakdowns take up only a small portion of the gap. This indicates that the increasing enhancement factor value with increasing P.D is dominated by the increase in surface area of the electrode with increasing P.D that adds new protrusions to the gap. Physically, this means that for the large gap sizes tested, increasing enhancement factor is likely dominated by changes in geometry *via* changes in P.D rather than breakdown induced changes at the surface. For the small gap sizes tested, SEM imaging shows that the surface is dominated by the creation and destruction of microprotrusions *via* breakdowns, which results in a gap that is significantly altered, and a surface that is smoothing. This behavior is represented by the decreasing enhancement factor with P.D. Physically, we see that for a gap that is dominated by variations in microprotrusions, the introduction of new protrusions with increasing P.D does little to increase the enhancement factor. Rather, the enhancement factor is dominated by significant alterations of the surface caused by many breakdowns.

The relationship between surface area and enhancement factor can be explored further by plotting the electrode surface area and enhancement factor versus the P.D for all gap sizes tested (Fig. 14). The change in the surface area values is minimal as the gap size decreases, since the gap size is small compared with the other dimensions, while the enhancement factor trends vary significantly. The surface area plots for each gap size are normalized to the enhancement factor at P.D of 2.5 mm (i.e., outside the region identified as "area effect" previously), and the slope represents the trend expected if the enhancement factor is dominated by the change in surface area.

For the 700-μm gap [Fig. 14(a)], the enhancement factor increases with P.D and follows closely to the increasing sur-

face area with P.D. As the gap size decreases, the measured enhancement factor continues to deviate further from the trend of the surface area [Fig. 14(b)–(e)]. This indicates that the surface area is a dominant driving factor for the enhancement factor value of the larger gaps, but plays an increasingly less significant role for smaller gaps. This is directly in line with the discussion and observations noted earlier.

IV. Conclusion

In this work, we have shown that the enhancement factor for a coaxial vacuum gap changes with varying gap sizes and P.Ds. This change is likely dominated by the electrode geometry, area of the penetrating electrode, and the creation and destruction of microprotrusions that are large compared with the cathode surface finish. Again, these are not the exclusive driving forces in changing the average enhancement factor value. Asymmetric distribution of breakdown in individual shots, a slightly varying work function, and conditioning of the electrode during the 50 shots all play a role in the enhancement factor value. Furthermore, due to the rep-rated nature of these experiments, the results may apply to single shot experiments.

For experiments on vacuum gaps of 150, 330, and 700 μm, we see an initial edge effect in the average enhancement factor with increasing P.D, followed by an increase at depths greater than 2.53 mm. This increasing in average enhancement factor is caused by an increase in microprotrusions that are likely due to the geometry of the electrode and the increase in area for breakdowns to occur. Where microprotrusions created by the explosive nature of breakdown formation in the vacuum gap remain small compared with the gap size and take up 40%–50% of the total surface area.

For 50- and 100-μm gap sizes, we see first that the average enhancement factor for these two gap sizes is smaller than the larger gap sizes tested for higher P.Ds. Second, we see the same edge effect behavior at a P.D smaller than 2.5 mm, after which there is a brief increase followed by a decrease in average enhancement factor with P.D. This behavior is likely due to the increased number of breakdowns creating and destroying microprotrusions and occupying a majority of the total surface area of the electrode. These are significant topological changes to the surface that occupy a majority of the gap. In the region of these changes, the increased number of overlapping breakdowns cause the surface to smooth, which leads to a decrease in microprotrusion height and enhancement factor. These trends are substantiated by imaging diagnostics.

Acknowledgment

Scanning electron microscope (SEM) imaging was performed in part at the San Diego Nanotechnology Infrastructure (SDNI) of University of California San Diego, a member of the National Nanotechnology Coordinated Infra-Structure (NNCI), which is supported by the National Science Foundation under Grant ECCS-1542148. SEM images were taken by Dr. Ryan Nicholl.

Data Availability

The data that support the findings of this study are available within the article. For further information, please contact the corresponding author.

References

[1] M. Okawa, T. Shioiri, H. Okubo, and S. Yanabu, "Area effect on electric breakdown of copper and stainless steel electrodes in vacuum," *IEEE Trans. Electr. Insul.*, vol. 23, no. 1, pp. 77–81, Feb. 1988.

[2] G. P. Beukema, "Conditioning of a vacuum gap by sparks and ion bombardment," *Physica*, vol. 61, no. 2, pp. 259–274, Sep. 1972.

[3] R. J. Harvey, R. A. Lee, A. J. Miller, and J. K. Wigmore, "Aspects of field emission from silicon diode arrays," *IEEE Trans. Electron Devices*, vol. 38, no. 10, pp. 2323–2328, Oct. 1991.

[4] D. Nicolaescu, "Physical basis for applying the Fowler–Nordheim J–E relationship to experimental I–V data," *J. Vac. Sci. Technol. B, Microelectron. Nanometer Struct.*, vol. 11, no. 2, p. 392, Mar. 1993.

[5] S. W. Cordaro and S. C. Bott-Suzuki, "Time and space resolved current density mapping in three dimensions using magnetic field probe array in a high voltage coaxial gap," *J. Appl. Phys.*, vol. 122, no. 21, Dec. 2017, Art. no. 213303.

[6] S. A. Slutz *et al.*, "Pulsed-power-driven cylindrical liner implosions of laser preheated fuel magnetized with an axial field," *Phys. Plasmas*, vol. 17, no. 5, May 2010, Art. no. 056303.

[7] R. H. Fowler and L. Nordheim, "Electron emission in intense electric fields," *Proc. R. Soc. Lond. A, Math. Phys. Sci.*, vol. 119, no. 781, pp. 173–181, May 1928.

[8] R. B. Marcus *et al.*, "Atomically sharp silicon and metal field emitters," *IEEE Trans. Electron Devices*, vol. 38, no. 10, pp. 2289–2293, Oct. 1991.

[9] T. E. Stern, B. S. Gossling, and R. H. Fowler, "Further studies in the emission of electrons from cold metals," *Proc. Roy. Soc. London A, Containing Papers Math. Phys. Character*, vol. 124, no. 795, p. 699, 1929.

[10] T. J. Lewis, "High field electron emission from irregular cathode surfaces," *J. Appl. Phys.*, vol. 26, no. 12, pp. 1405–1410, Dec. 1955.

[11] A. G. Mesyats, *Cathode Phenomena in a Vacuum Discharge: The Breakdown, the Spark and the Arc*. Moscow, Russia: Nauka, 2000.

[12] E. A. Litvinov, G. A. Mesyats, and A. G. Parfenov, "The nature of explosive electron emission," *Sov. Phys.-Doklady*, vol. 28, no. 3, pp. 1019–1020, 1983.

[13] G. A. Mesyats, "Ecton mechanism of the vacuum arc cathode spot," *IEEE Trans. Plasma Sci.*, vol. 23, no. 6, pp. 879–883, Dec. 1995.

[14] J. E. Daalder, "Cathode erosion of metal vapour arcs in vacuum," M.S. thesis, Dept. Elect. Eng., Eindhoven Univ. Technol., Eindhoven The Netherlands, 1978.

[15] B. Jüttner, "Erosion craters and arc cathode spots in vacuum," *Beitir. Plasma Phys.*, vol. 19, no. 1, pp. 25–48, 1979.